Millimeter-Long Carbon Nanotubes: Outstanding Electron-Emitting Sources

Néstor Perea-López,[†,‡] Bernabé Rebollo-Plata,[‡] Juan Antonio Briones-León,[‡] Aarón Morelos-Gómez,[‡] Daniel Hernández-Cruz,[‡] Gustavo A. Hirata,[§] Vincent Meunier,[⊥] Andrés R. Botello-Méndez,[∥] Jean-Christophe Charlier,[∥] Benji Maruyama,[#] Emilio Muñoz-Sandoval,[‡] Florentino López-Urías,[‡] Mauricio Terrones,[†,▽,*] and Humberto Terrones[∥,△]

[†]Department of Physics, The Pennsylvania State University, 104 Davey Lab, University Park, Pennsylvania 16802-6300, United States, [‡]Advanced Materials Department, IPICYT, Camino a la Presa San José 2055, Lomas 4a. Sección, San Luis Potosí 78216, México, [§]Center for Nanoscience and Nanotechnology-UNAM, Km 107 Carretera Tijuana-Ensenada, Ensenada, B. C, 22860, México, [⊥]Department of Physics, Rensselaer Polytechnic Institute, Troy, New York 12280, United States, [∥]Institute of Condensed Matter and Nanosciences, Université Catholique de Louvain, Place Croix du Sud 1 (NAPS-Boltzmann), B-1348 Louvain-la-Neuve, Belgium, [#]Air Force Research Laboratory, Materials and Manufacturing Directorate, AFRL/RX, Wright-Patterson Air Force Base, Ohio 45433, United States, [△]Oak Ridge National Laboratory, One Bethel Valley Road, Oak Ridge, Tennessee 37831-6367, United States, and [▽]Department of Physics, Department of Materials Science and Engineering, and Materials Research Institute, The Pennsylvania State University, University Park, Pennsylvania 16802-6300, United States, and Research Center for Exotic Nanocarbons (JST), Shinshu University, Wakasato 4-17-1, Nagano 380-8553, Japan

ABSTRACT We are reporting the fabrication of a very efficient electron source using millimeter-long and highly crystalline carbon nanotubes. These devices start to emit electrons at fields as low as 0.17 V/μm and reach threshold emission at 0.24 V/μm. In addition, these electron sources are very stable and can achieve a peak current density of 750 mA cm^{-2} at only 0.45 V/μm. In order to demonstrate intense electron beam generation, these devices were used to produce visible light by cathodoluminescence. Finally, density functional theory calculations were used to rationalize the measured electronic field emission properties in open carbon nanotubes of different lengths. The modeling establishes a clear correlation between length and field enhancement factor.

KEYWORDS: field emission · carbon nanotube · low field · very long nanotubes

Electron field emission (FE) from cold cathodes has attracted the attention of numerous scientists after the bulk production of multiwalled carbon nanotubes. In this respect, de Heer *et al*. in 1995 demonstrated that aligned carbon nanotubes (CNTs) could emit electrons from their polarized tips.[1] In general, CNT emitters require relatively low electric fields for achieving the turn-on emission (E_{ON}) and threshold emission (E_{Th}). E_{ON} and E_{Th} were defined as the electric fields that generate the current densities J_{ON} = 10 μAcm^{-2} and J_{Th} = 10 mA cm^{-2}, respectively.[2] From an application point of view, E_{Th} is an important parameter of an electron-emitting device because it is directly related to the device power consumption at operation conditions, while E_{ON} is the electric field at which field emission initiates. Existing CNT-based field emitters (CNT-FEs) exhibit E_{ON} between 0.6 and 2 V/μm,[1−7] values that are superior when compared to other materials such as W tips or ZnO nanowires,[8] both with E_{ON} > 6 V/μm. To date, the lowest turn-on electric field reported for a CNT-FE is 0.6 V/μm,[2] while E_{Th} can be between 2 and 30 V/μm.[3−6] In addition, CNT-FEs possess other excellent properties related to their chemical and thermal stability at relatively high temperatures (~500 °C). On the basis of these characteristics, CNT-FEs have been used in the fabrication of flat panel displays, light bulbs, and compact X-ray sources.[4−6]

RESULTS AND DISCUSSION

Figure 1 shows the *I*−*E* curve of the 2 mm long CNT pillar electron source that exhibits very step-like behavior and emission current as high as 100 μA; the inset shows the *J*−*E* plot of the 2 mm device. In general, below 0.17 V/μm the contributions of the noise and the dark current can be observed, but above 0.17 V/μm, the steep contribution of the field emission current is evident. Within this region, the milestone value threshold current density (J_{Th} = 10 mA cm^{-2}) is labeled, and it is remarkable that the emitter reached such a current density at only ~0.24 V/μm. A higher current density of 100 mA/cm^2 ($J \gg J_{Th}$) was achieved at a field as low as ~0.28 V/μm. This is an outstanding value, considering that all the so far reported emitters do not present any electron emission at such low electric fields. Furthermore, we explored the limits of emission current, finding current saturation above 220 μA; at such a

* Address correspondence to mtterrones@shinshu-u.ac.jp; mut11@psu.edu; mtterrones@gmail.com.

Received for review March 27, 2011 and accepted May 24, 2011.

Published online May 25, 2011
10.1021/nn201149y

current, arc breakdown was observed in the system. The highest field emission current density achieved was ~750 mA cm^{-2} at only 0.45 V/μm. On the other end, the dark current in reverse bias was also measured, finding a linear behavior at a reverse field between 0 and 0.50 V/μm, reaching a maximum current of 28 nA.

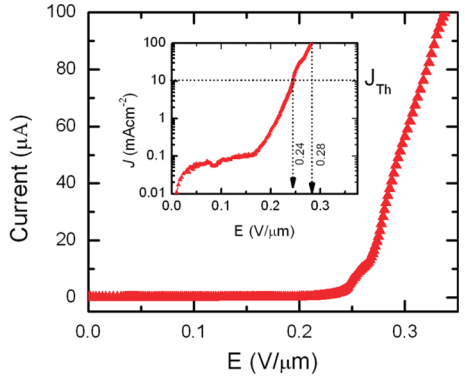

Figure 1. *I*–*E* characteristic of the 2 mm long electron source in the μA range current region showing very step-like behavior. In the inset is the *J*–*E* plot with logarithmic current density (*J*) axis. It can be seen that field emission current starts barely after 0.17 V/μm. The field to achieve J_{Th} was only 0.24 V/μm and a 10 times higher current density of only 0.28 V/μm. Emitter cross section area, $A \approx 3.14 \times 10^{-4}$ cm^2, was used for the calculation of *J*.

In order to distinguish the influence of the CNT pillar length on the FE properties of our emitters, a comparison was made between 1 mm and 2 mm long pillars. We found a great improvement in the FE properties for the longer emitter (2 mm). The *J*–*E* curves for both lengths are shown in Figure 2a. Additionally, in Figure 2b the Fowler–Nordheim (F–N) plots for these data show linear behavior in the region $E_{Th} > E_{app} > E_{ON}$ and confirm electron field emission by tunneling electrons from the CNTs to the vacuum when applying an electric field. Nevertheless, in the F–N plots it is possible to notice slight deviations from linearity, especially at the high electric field end, where the contribution of emission spots located at different heights affect the total emission current; this is an effect commonly observed in large-area emitters.[9,10]

From the F–N model, it is possible to obtain the field enhancement factor, β. This factor relates the local field at the emitter tip, E_{loc}, and the macroscopic field ($E_{macro} = V/d$) by the expression $E_{loc} = \beta E_{macro}$. Experimentally, β can be obtained by measuring the slope, *s*, of the linear region in the F–N plot by using the expression

$$\beta = -B\phi^{3/2}d/s$$

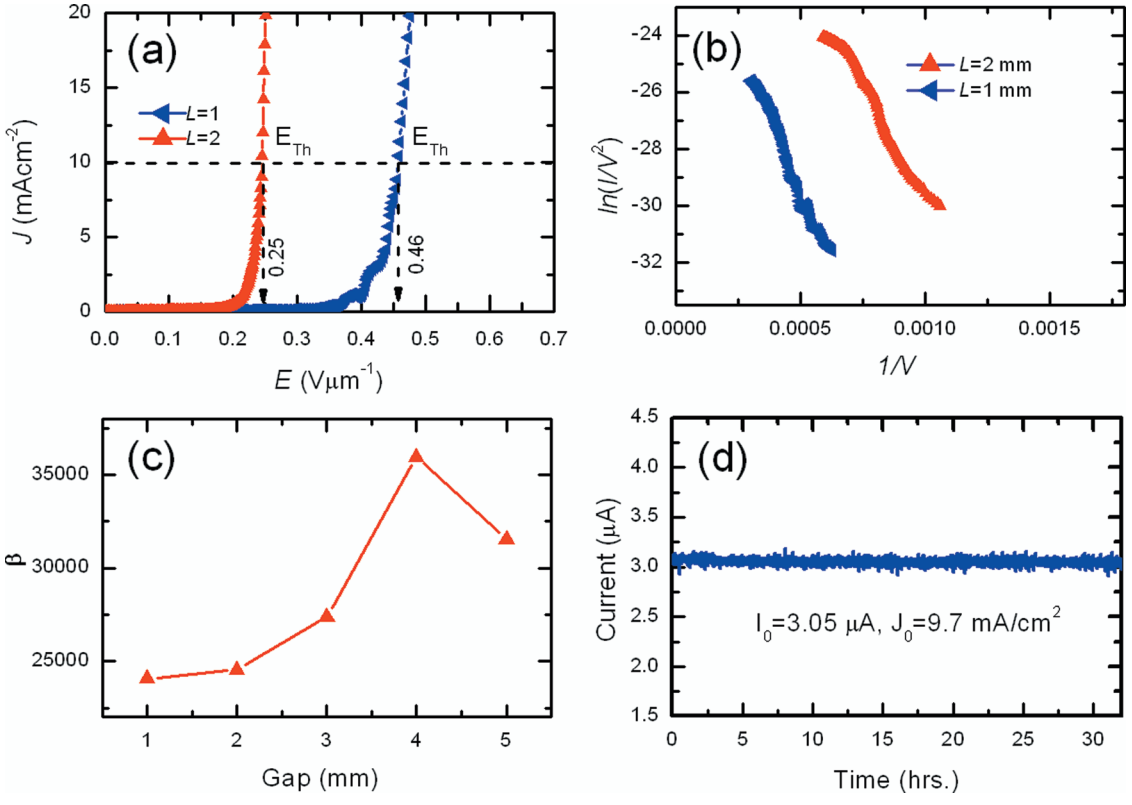

Figure 2. (a) *J*–*E* curves of two field emitters constructed with pillars of 2 mm and 1 mm long where the milestone value E_{Thr} is labeled. (b) Fowler–Nordheim plots created with the same data presenting different slopes for each emitter, and linear behavior in the electron emission region. (c) Variation of the field enhancement factor as the vacuum gap, *d*, goes from 1 mm to 5 mm for the 2 mm long emitter pillar. (d) Current *vs* time plot. The current fluctuates ±3% from the set point value $I_0 = 3.05$ μA.

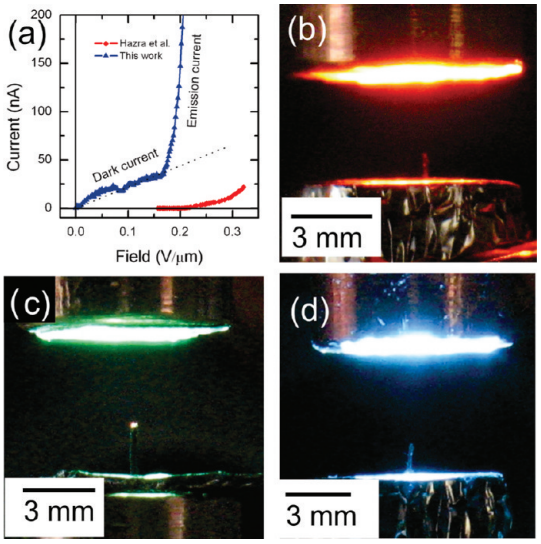

Figure 3. Comparison between the best emitter reported by Hazra *et al*. and the 2 mm device reported in this work. (a) *I*−*E* plots of both devices. Visible light emitted by CL from (b) Y_2O_3:Eu for red, (c) $EuAl_2O_4$ for green, and (d) Sr_2CeO_4 for blue; all the phosphor oxide powders were excited using the electron sources reported here.

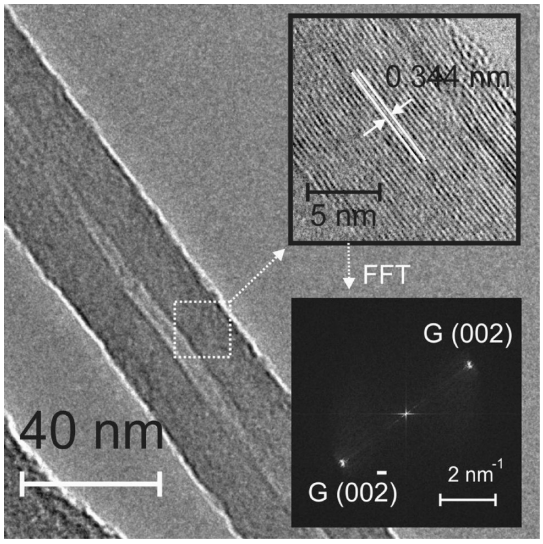

Figure 4. HRTEM micrograph of a pristine CNT belonging to a pillar. In the top inset a HRTEM image reveals that the walls are formed by high-quality graphitic planes, and well-defined graphite spots can be observed in the FFT inset shown below.

where the constant $B = 6.83 \times 10^9$ V eV$^{-3/2}$ m^{-1}, ϕ is the work function, and d is the electrode separation distance.[11] Assuming $\phi = 5$ eV, the same as graphite, and $d = 5$ mm, β results in very large values of $\sim 3.2 \times 10^4$ for the 2 mm long and $\sim 1.8 \times 10^4$ for 1 mm long CNT pillars at vacuum gaps of 5 mm; such values are among the largest reported so far.[12]

Zhong *et al*.[13] observed that the field enhancement factor depends on the vacuum gap. Such a result indicates that for the same emitter, β and the characteristic threshold and turn-on fields are influenced by the device geometry and are not an intrinsic property of the emitter; thus these authors proposed a two-region field-emission (TRFE) model for CNT emitters where both the vacuum gap and the emitter length are considered in the calculation of β, finding a linear relationship established between $1/\beta$ and 1/d when $L \ll d$. Nevertheless, in our case, in which very long nanotubes were used, $L \approx d$, such a behavior was not observed. Instead we found a maximum value for β for a specific d value, as observed in Figure 2c. A similar behavior was recently reported by Tseng *et al*., who also discussed the dependence of β in terms of two non-uniform electric field distribution areas similar to the TRFE model.[14] One interesting observation in our system is the fact that if we use the mean macroscopic electric field ($E_0 = V/L + d$) across both electrodes, including the emitter length, in order to plot the current density, J *vs* E_0, all graphs lie very close to each other, exhibiting the same E_{ON} for all measured vacuum gaps. Therefore, further investigation is required in order to explain such a behavior; these plots are presented only as Supporting Information in Figure S1.

Once we found good emission properties on these CNT emitters, we proceeded to test emission stability. These measurements were performed on the 2 mm device, finding a current variation in the range of ±3% of the mean value of 3.05 μA (Figure 2d). These devices were thoroughly tested, by accumulating tens of hours of operation. The electron emission properties were found not to disappear on any of them.

Recently, Hazra *et al*. reported field emission from CNT microarrays at very low onset electric fields.[15] Nevertheless, the emission current generated with those devices barely exceeded the dark current range (nA). A comparison of the data reported by Hazra *et al*. and the device reported here is shown in Figure 3a. Although Hazra *et al*. reported very high current density ($\sim$3 A/cm^2) from their emitter, the maximum current produced by their device reached only 20 nA,[16] and our device was capable of producing 4 orders of magnitude more current (1×10^5 nA). In addition, using our electron sources, we generated intense light emission from red (Y_2O_3:Eu), green ($EuAl_2O_4$), and blue (Sr_2CeO_4) phosphor powders excited by cathodoluminescence (CL); photographs of these experiments are shown in Figures 3b−d. For such a purpose, the phosphor powders were ultrasonically dispersed in ethanol, poured directly drop-by-drop in order to form a uniform coat on the anode plate, and allowed to dry. Extremely bright light emission characteristics of each phosphor material were observed at relatively low electron energies between 0.5 and 2 keV; such values rely on the excitation cross section for electrons inherent to each phosphor material.[17−19] Therefore, the CNT pillars reported in this article could be used in devices such as very large area flat-panel displays or large-area low-voltage lamps.

TABLE 1. Results of XPS C_{1s} Quotient of the Sum of Oxidized Groups Divided by the Sum of All Carbons Detected in CNTs Synthesised by CVD with and without Ethanol

carbon coordination	no ethanol in CVD	ethanol in CVD
sp^2	67.0	75.3
sp^3	19.6	10.9
C—O	2.3	5.8
C═O	3.7	6.4
COO	2.4	1.6
[C(O)]/[C]	8.9	13.8

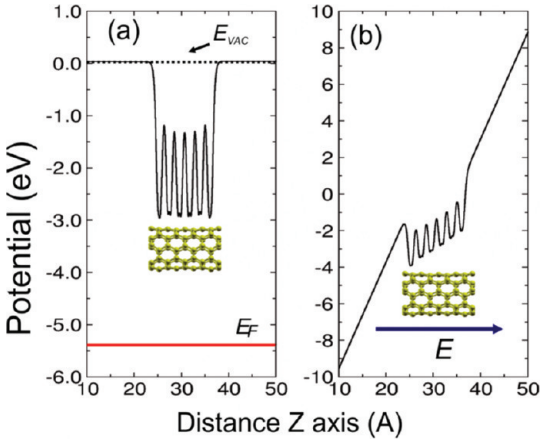

Figure 5. Macroscopic average of a (5,5) CNT (a) in the absence of electric field and (b) in the presence of an electric field. The work function (ϕ) is calculated as $\phi = E_{vac} - E_F$.

To the best of our knowledge, we have now used the longest CNTs pillars to create an efficient electron source, but we should also note that Pan *et al*. reported the use of long nanotubes in field emission experiments.[2] Unfortunately, in their approach a small portion of a continuous forest of long nanotubes (possibly irregular and with lower crystallinity) was detached and used as electron source, in contrast to our approach, in which we have regular pillars grown independently on patterned substrates. High-resolution transmission electron microscopy (HRTEM) analysis of the CNTs grown on pillars is presented in Figure 4 and reveals their high degree of crystallinity. CNT crystalline quality is affected when very long periods of growth are used to grow very long carbon nanotubes;[20] hence, it is very likely to find fewer defects in our long pillars, grown for 4 h. The CNT forests used by Pan *et al*. grew during 48 h.[2] In consequence, along with the pillar length, crystalline quality is also an important factor that promotes enhanced performance in CNT electron sources. Such differences are clearly reflected in the better emission properties found in this work.

Continuing with the study of the crystalline quality of the CNTs used in our emitters, we explored the effect of ethanol on the quality of the CNTs. For this purpose, XPS measurements were performed on CNTs synthesized

TABLE 2. Electronic and FE Properties for the Open (5,5) CNTs for Three Different Lengths[a]

cnt length	E_F (eV)	E_{vac} (eV)	ϕ (eV)	β	E_b (eV)
9.85 Å (90 atoms)	−4.65	−0.02	4.63	1.10	−8.55
14.78 Å (130 atoms)	−4.63	−0.02	4.61	1.19	−8.69
17.24 Å (150 atoms)	−4.61	−0.02	4.59	1.56	−8.74

[a] The values shown correspond to the Fermi level (E_F), electrostatic potential (E_{vac}), work function (ϕ), field enhancement factor (β), and binding energy (E_b).

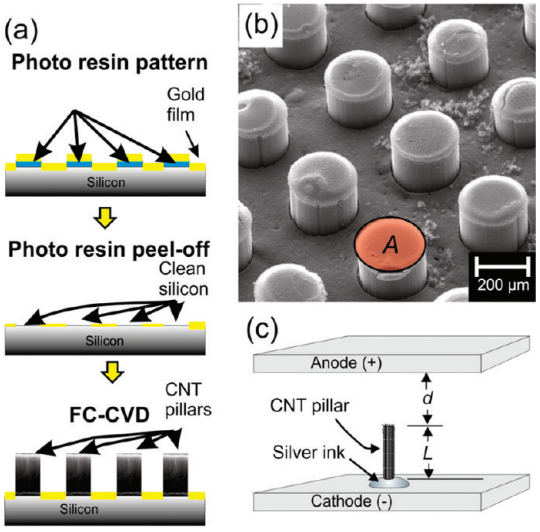

Figure 6. (a) Key steps for CNT pillar growth; (b) morphology of a finished CNT pillar array; and (c) schematic representation of the emitter device.

with and without ethanol during CVD. A quantitative analysis of the carbon—oxygen groups of each sample was created. Table 1 shows the C_{1s} binding energies from XPS caused by the interaction of oxygen and carbon atoms. The nanotubes extracted from our pillars revealed a dominant presence of sp^2-hybridized carbon atoms (graphitic carbon), consequently exhibiting a lower concentration of sp^3-hybridized carbons (defects).

In order to further understand the effect of nanotube length on the field emission properties, first-principles theoretical calculations were performed using the SIESTA code[21] to study open CNTs of different lengths (calculation details are provided in the Supporting Information, S2). The electron field emission properties were investigated with and without an external electric field. In the absence of an electric field, the work function (ϕ) can be estimated by $\phi = E_{vac} - E_F$, where E_{vac} is the electrostatic potential in the vacuum and E_F is the Fermi energy. ϕ is interpreted as the minimum energy required for an electron to be removed from the carbon nanotube to the vacuum level.[22] In our calculations, the vacuum level is determined by the plateau value of the macroscopic average of the planar surface electrostatic potential outside the nanotube.[23] In the presence of an applied electric field (E_{app}), the emission properties were obtained using the field enhancement factor (β), which is given by

$\beta = E_{loc}/E_{app}$, where E_{loc} corresponds to the local field and is estimated from the slope of the electrostatic potential.[24]

Figure 5 presents the macroscopic average of the surface electrostatic potential of a (5,5) carbon nanotube. The cell parameters were carefully chosen to ensure that the electrostatic potential was constant (E_{vac}) outside the nanotube. At the same time, characteristic oscillations were observed inside the nanotube due to the presence of atomic details on the nanotube surface. In this way, the electrostatic potential along the nanotube axis in the absence of an external electric field was calculated (see Figure 5a). In addition, the effect of an applied electric field was considered. Here, the macroscopic average of the surface electrostatic potential exhibited a linear behavior (see Figure 5b). The slope of the straight line was associated with E_{loc}.

Furthermore, in order to study the length dependence of the FE properties, we performed calculations on (5,5) nanotubes of three different lengths. The longest nanotubes exhibit a zero electronic gap at low electric fields, which could be related to a smaller E_{ON} observed in long CNTs. Both ϕ and β values are summarized in Table 2. Note that ϕ decreases as the nanotube length increases. A small ϕ and a large β are both needed for an improved FE behavior. Small ϕ means the electrons are released easily, and large β increases the local field in the CNT tips.

CONCLUSIONS

The outstanding electric properties of these CNT electron sources are mainly due to the following parameters: (a) millimeter length, which creates a huge aspect ratio, which, in turn, increases the field enhancement factor for the Fowler–Nordheim emission; (b) the high degree of crystallinity within the emitting tubes, which reduces electron scattering and hence electric resistance. Both properties are promoted by the use of small amounts of ethanol in the CNT synthesis.[25] In addition, the calculations of the electronic and FE properties of CNTs with three different lengths were compared. It was found that the longest CNT has a smaller work function and larger β, which are responsible for FE improvement, a result that is in agreement with our experimental results.

MATERIALS AND METHODS

Millimeter-long carbon nanotubes were produced by a floating catalyst CVD process using ferrocene (2.5 wt %) as iron catalyst source, toluene (97 wt %) as carbon source, and ethanol (0.5 wt %) as oxygen source. The addition of ethanol is intended to promote the faster formation of longer nanotubes; the process has been explained in detail by Botello-Mendez *et al.*[25] In this particular case, the silicon substrates were patterned with a photoresin mask (MicroChem SU8-2015) and covered with a 50 nm thick gold film deposited by dc sputtering. Subsequently, the patterned photoresin layer was peeled off to expose circular areas of clean silicon, while the rest of the substrate retained the gold film in order to inhibit CNT growth (Figure 6a). The diameter of the pillars is defined by the size of the circular pattern, while their length (L) is controlled by the CVD growing time (Figure 6b). The CNT pillars used in this work were ~100 μm in radius and grown during different time periods to have straight 1 mm and 2 mm long samples. It is possible to grow pillars shorter in diameter and longer than 2 mm; however such samples were not used for FE experiments because those dimensions produced curved pillars.

The CNT-based electron sources are constructed by placing an individual pillar on a metallic plate using a small drop of silver ink, as depicted in Figure 6c. The CNT pillars must be detached from the growth substrate (see Figure 6b) using precision tweezers. Then, we placed the pillar onto the metallic plate in such a way that the pillar base acts as an emitter tip. In that way, the open nanotube edges created by the detachment from the substrate can act as emitter point (see Supporting Information, S3).

The J–E electrical characteristics of the CNT-FEs were measured at room temperature under ~133×10^{-6} Pa vacuum conditions. The emission current (I) was measured with a picoammeter (Keithley model 6485) connected in series with the emitter. The voltage was supplied by a dc high-voltage power supply (V_{app}) and measured with a voltmeter. For the field emission measurements, the cathode had a fixed position and the anode was moved up and down with a stepper motor (Huntington Lab, SSP 600) with step size of 15 μm in order to set the tip to anode separation distance, d, at a desired distance. The tip–anode separation, d, was used to calculate the macroscopic electric field, $E = V/d$, and the current density, $J = I/A$, where A is the emitter cross section area in cm^{-2} (see Figure 6b and c).

Acknowledgment. We thank D. Ramírez, F. Tristán, S. Vega, G. Labrada, and B. Rivera for technical support. M.T. thanks JST-Japan for funding the Research Center for Exotic NanoCarbons, under the Japanese Regional Innovation Strategy Program by the Excellence. H.T. acknowledges support as visiting professor from the Ecole Polytechnique of Louvain and as a visiting scientist at the CNMS of ORNL. J.C.C. acknowledges the FNRS of Belgium. We also thank the Air Force Research Laboratory for partial support of this work, grant FA9550-08-1-0204. A.R.B.M. is indebted to the M. De Merre Prize of Louvain. This work was also supported in part by CONACYT-México grants: Fondo Mixto de San Luis Potosí 63001 S-3908 and 63072 S-3909 (E.M.S.), 60218-F1 (F.L.U.), 48300 (E.M.S.), and postdoctoral fellowship (N.P.L.).

Supporting Information Available: S1: J–E curves for different vacuum gaps, S2: SIESTA code calculation details, S3: Microanalysis of the CNT open tips. This material is available free of charge *via* the Internet at http://pubs.acs.org.

REFERENCES AND NOTES

1. de Heer, W. A.; Chatelain, A.; Ugarte, D. A Carbon Nanotube Field-Emission Electron Source. *Science* **1995**, *270*, 1179–1181.
2. Pan, Z. W.; Frederick, C. K.; Au, K.; Lai, H. L.; Zhou, W. Y.; Sun, L. F.; Liu, Z. Q.; Tang, D. S.; Lee, C. S.; Lee, S. T.; *et al*. Very Low-Field Emission from Aligned and Opened Carbon Nanotube Arrays. *J. Phys. Chem. B* **2001**, *105*, 1519–1522.
3. Kuznetzov, A. A.; Lee, S. B.; Zhang, M.; Baughman, R. H.; Zakhidov, A. A. Electron Field Emission from Transparent Multiwalled Carbon Nanotube Sheets for Inverted Field Emission Displays. *Carbon* **2010**, *48*, 41–46.
4. Choi, W. B.; Chung, D. S.; Kang, J. H.; Kim, H. Y.; Jin, Y. W.; Han, I. T.; Lee, Y. H.; Jung, J. E.; Lee, N. S.; Park, G. S.; *et al*. Fully Sealed, High-Brightness Carbon-Nanotube Field-Emission Display. *Appl. Phys. Lett.* **1999**, *75*, 3129–3131.
5. Murakami, H.; Hirakawa, M.; Tanaka, C.; Yamakawa, H. Field Emission from Well-Aligned, Patterned, Carbon Nanotube Emitters. *Appl. Phys. Lett.* **2000**, *76*, 1776–1778.

6. Calderón-Colón, X.; Geng, H.; Gao, B.; An, L.; Cao, G.; Zhou, O. A Carbon Nanotube Field Emission Cathode with High Current Density and Long-Term Stability. *Nanotechnology* **2009**, *20*, 325707-1–325707-5.
7. Manohara, H. M.; Bronikowski, M. J.; Hoenk, M.; Hunt, B. D.; Siegel, P. H. High-Current-Density Field Emitters Based on Arrays of Carbon Nanotube Bundles. *J. Vac. Sci. Technol., B: Microelectron. Nanometer Struct.--Process., Meas., Phenom.* **2005**, *23*, 157–161.
8. Lee, C. J.; Lee, T. J.; Lyu, S. C.; Zhang, Y.; Ruh, H.; Lee, H. J. Field Emission from Well-Aligned Zinc Oxide Nanowires Grown at Low Temperature. *Appl. Phys. Lett.* **2002**, *81*, 3648–3650.
9. Bonard, J. M.; Dean, K. A.; Coll, B. F.; Klinke, C. Field Emission of Individual Carbon Nanotubes in the Scanning Electron Microscope. *Phys. Rev. Lett.* **2002**, *89*, 197602-1–197602-4.
10. Manohara, H. M.; Toda, R.; Lin, R. H.; Liao, A.; Bronikowski, M. J.; Siegel, P. H. Carbon Nanotube Bundle Array Cold Cathodes for THz Vacuum Tube Sources. *J. Infrared, Millimeter, Terahertz Waves* **2009**, *30*, 1338–1350.
11. Gao, H.; Mu, C.; Wang, F.; Xu, D.; Wu, K.; Xie, Y.; Liu, S.; Wang, E.; Xu, J.; Yu, D. Field Emission of Large-Area and Graphitized Carbon Nanotube Array on Anodic Aluminum Oxide Template. *J. Appl. Phys.* **2003**, *93*, 5602–5605.
12. Jung, Y. J.; Kar, S.; Talapatra, S.; Soldano, C.; Viswanathan, G.; Li, X.; Ou, F. S.; Avadhanula, A.; Vajtai, R.; Curran, S.; *et al*. Aligned Carbon Nanotube-Polymer Hybrid Architectures for Diverse Flexible Electronic Applications. *Nano Lett.* **2006**, *6*, 413–418.
13. Zhong, D. Y.; Zhang, G. Y.; Liu, S.; Sakurai, T.; Wang, E. G. Universal Field-Emission Model for Carbon Nanotubes on a Metal Tip. *Appl. Phys. Lett.* **2002**, *80*, 506–508.
14. Tseng, S.; Yao, B.; Tsai, C. Field Emission from Individual Free-Standing Carbon Nanotubes. *Jpn. J. Appl. Phys.* **2010**, *49*, 105101-1–105101-4.
15. Hazra, K. S.; Rai, P.; Mohapatra, D. R.; Kulshrestha, N.; Bajpai, R.; Roy, S.; Misra, D. S. Dramatic Enhancement of the Emission Current Density from Carbon Nanotube Based Nanosize Tips with Extremely Low Onset Fields. *ACS Nano* **2009**, *3*, 2617–2622.
16. The data were digitized from Figure 3d in Hazra *et al*. using Plot Digitizer software.
17. McKittrick, J.; Bacalski, C. F.; Hirata, G. A.; Hubbard, K. M.; Pattillo, S. G.; Salazar, K. V.; Trkula, M. Characterization of Photoluminescent $(Y_{1-x}Eu_x)_{(2)}O_3$ Thin Films Prepared by Metallorganic Chemical Vapor Deposition. *J. Am. Ceram. Soc.* **2000**, *83*, 1241–1246.
18. Rakov, N.; Ramos, F. E.; Hirata, G.; Xiao, M. Strong Photoluminescence and Cathodoluminescence Due to f-f Transitions in Eu^{3+} Doped Al_2O_3 Powders Prepared by Direct Combustion Synthesis and Thin Films Deposited by Laser Ablation. *Appl. Phys. Lett.* **2003**, *83*, 272–274.
19. Danielson, E.; Devenney, M.; Giaquinta, D. M.; Golden, J. H.; Haushalter, R. C.; McFarland, E. W.; Poojary, D. M.; Reaves, C. M.; Weinberg, W. H.; Wu, X. D. A Rare-Earth Phosphor Containing One-Dimensional Chains Identified Through Combinatorial Methods. *Science* **1998**, *279*, 837–839.
20. Li, X.; Zhang, X.; Ci, L.; Shah, R.; Wolfe, C.; Kar, S.; Talapatra, S.; Ajayan, P. M. Air-Assisted Growth of Ultra-Long Carbon Nanotube Bundles. *Nanotechnology* **2008**, *19*, 455609-1–455609-7.
21. Soler, J. M.; Artacho, E.; Gale, J. D.; García, A.; Junquera, J.; Ordejón, P.; Sánchez-Portal, J. D. The SIESTA Method for Ab Initio Order-N Materials Simulation. *Phys. Condens. Matter* **2002**, *14*, 2745–2779.
22. Schulte, F. K. On the Theory of the Work Function. *Z. Phys. B: Condens. Matter* **1977**, *27*, 303–307.
23. Baldereschi, A.; Baroni, S.; Resta, R. Band Offsets in Lattice-Matched Heterojunctions: A Model and First-Principles Calculations for GaAs/AlAs. *Phys. Rev. Lett.* **1988**, *61*, 734–735.
24. Meunier, V.; Roland, C.; Bernholc, J.; Nardelli, M. B. Electronic and Field Emission Properties of Boron Nitride/Carbon Nanotube Superlattices. *Appl. Phys. Lett.* **2002**, *81*, 46–48.
25. Botello-Méndez, A. R.; Campos-Delgado, J.; Morelos-Gómez, A.; Romo-Herrera, J. M.; Rodríguez, A. G.; Navarro, H.; Vidal, M. A.; Terrones, H.; Terrones, M. Controlling the Dimensions, Reactivity and Crystallinity of Multiwalled Carbon Nanotubes Using Low Ethanol Concentrations. *Chem. Phys. Lett.* **2008**, *453*, 55–61.